EBSD study of early fractured phenomena in a 350 grade Maraging steel elbows exposed to hydrofluoric acid

Mohammad Masoumi[a,*], Hamilton F.G. Abreu[b], Luiz F.G. Herculano[b],
Juan M. Pardal[c], Sérgio S.M. Tavares[d], Marcelo J.G. Silva[b]

[a] *Universidade Federal do ABC, Centro de Engenharia, Modelagem e Ciências Sociais Aplicadas, Av. dos Estados, 5001 – Bangú, 09210-580 Santo André, SP, Brazil*
[b] *Universidade Federal do Ceará (UFC), Centro de Tecnologia, Departamento de Engenharia Metalúrgica e de Materiais, Fortaleza, CE, Brazil*
[c] *Universidade Federal Fluminense (UFF), Programas de Pós-Graduação em Engenharia Mecânica (PGMEC) e Montagem Industrial, Rua Passo da Pátria, 156, CEP 24210-240, Niterói, RJ, Brazil*
[d] *Centro Federal de Educação Celso Suckow, Programa de Pós-Graduação em Engenharia Mecânica e Tecnologia de Materiais, Rio de Janeiro, RJ, Brazil*

ARTICLE INFO

ABSTRACT

The effect of grain orientations, boundary characteristics, and crystal effects on the crack formation of a 350 high strength Maraging steel elbows exposed to hydrofluoric acid was investigated in the present research. Tempered low tetragonal martensite and fresh martensite were characterized by scanning electron microcopy. Moreover, no segregation zone and precipitates were found near the crack path. Detail analyzing the spatial distribution of crystal orientations by electron backscattered diffraction technique revealed the development of two soft and hard grains. Soft grains oriented approximately along {110} planes provide adequate slip systems to promote dislocation mobility, indicating as low Taylor factor grains distributed well the strain gradient. However, hard grains associated with low compact {001} planes decrease dislocation mobility and increasing the strain accumulation. Micro-cracks initiation and propagation along these high internal energy grains are expected consequently.

1. Introduction

The development of advanced applications of structural materials having superior mechanical properties (i.e., high strength and toughness) and corrosion resistance for advanced applications was introduced in the study of Maraging steels by Bieber in the late 1950s [1]. The benefits of low carbon content in high nickel Maraging steels are guaranteed to spread the application of these steels, regardless of the high price of the alloying elements. In addition, Jones et al. [2] and Li et al. [3] reported that in the iron–nickel binary system, the austenite to martensite transformation is of a diffusionless type. Thus, martensite develops at all cooling rates. High nickel Maraging steels with advanced high-strength (yield stress > 248 KSI (1700 MPa)) and low carbon content are already widely used in high pressure/temperature systems. Solution annealing at temperatures about 760–870 °C, followed by rapid cooling to achieve martensitic structure, and finally aging treatment in the range of 460–540 °C is a common heat treatment of Maraging steel. Precipitates hardeners (such as Ni_3Mo, Ni_3Ti, Ni_3V, $Fe_2(Mo,Ti)$, etc) formed during aging treatment are responsible for superior

---

mechanical properties [4–8].

Although several metallurgical methods, such as altering solution and aging treatments time and temperature [3,5], controlling of the chemical composition [4], avoiding the formation of segregation zones and precipitates growing [7], controlling the microstructure [9], and strain hardening [8,10] have been studied to increase fracture toughness and optimize the service life of application in a server environment, these methods cannot eliminate totally undesirable failures. Therefore, in the last decade, a new method based on crystallographic parameters (i.e., grain orientation, crystal misorientation, grain boundary types, and crystal defects) was introduced to improve ductility and fracture toughness. Crack paths containing (crack initiation, trajectory, and tip) were analyzed in several researches [11–13]. The results revealed that grains orientated along {001} planes parallel to normal direction (ND) are highly susceptible for crack propagation. Blondé et al. [14] analyzed the accumulation of lattice plane strain in grains oriented along specific {hkl} planes using in situ high-energy X-ray diffraction under uniaxial loading. They reported the gradual increasing in elastic and yield response by means of the orientation dependence as a function of interatomic distance, i.e., $E_{(100)} \ll E_{(102)} < E_{(111)} < E_{(112)} < E_{(110)}$ [15].

Electron backscattered diffraction (EBSD) is a powerful method for plasticity characterization and can be widely used in failure analysis of polycrystalline materials. EBSD installed in a scanning electron microscope (SEM) can measure crystal orientation and local strain gradient in the sample. As a general description, monochromatic electrons emitted from the SEM probe to the sample form Kikuchi bands according to the diffraction criteria for the crystal [16,17]. EBSD detector is centered in the Kikuchi bands formed by this technique, then, it can be analyzed to provide the high accuracy orientation of the diffracting crystal relative to the detector [18]. The plasticity behaviour in polycrystalline materials can be controlled by dislocation multiplication and lattice distortion inside the grain. Detailed EBSD misorientation analysis on the crack trajectory is an important procedure for the failure analysis of post-mortem after failure [18].

In the present paper, microstructure and failure analysis were studied regarding a fractured 350 grade maraging elbow under service in parts operating under stress in an environment with traces of hydrofluoric acid,. No evidence provided by common micrograph studies was considered to explain early fracture. However, the importance of crystallographic analyses such as grain orientation, crystal misorientation, grain boundary types, and crystal defects has been emphasized for failure analysis methods.

2. Material and methodology

A fractured elbow 350 grade Maraging steel under service in parts operating under stress in an environment with traces of hydrofluoric acid in support of the molten salt reactor experiment conversion project was studied in the present research. The chemical composition of the investigated material was measured using optical emission spectroscopy listed in Table 1.

A rectangular sample of about $10 \times 10 \times 2$ mm was removed from the as-received sample, then ground to # 1200 to employ of analyzing X-ray diffraction (XRD). XRD analysis was performed using a Philips X'Pert X-ray diffractometer using a Cu X-ray emitter at 40 kV and 45 mA. The diffraction peaks were obtained at the incident angle between 35 and 95°, with a step interval of 0.013° and a scan rate of 0.5°/min.

Scanning electron microscopy (SEM) analyzing was conducted using a FEI Quanta 450 FEG on the surface plane of the investigated material. The samples were ground and polished following the standard metallographic preparation procedure, then, the samples were etched with an ammonium persulfate $((NH_4)_2S_2O_8)$ reagent to reveal the structure. Micro-Vickers hardness tests were also performed according to ASTM C1327 on polished samples using a diamond indenter and 9.807 N loads for Vickers indentations (HMV2 Series – Shimadzu Machine) with a dwell time of 15 s. The average value was determined from ten indents of the sample.

Finally, electron backscattered diffraction (EBSD) measurements were performed on a field emission SEM (FEI XL30) operating at an acceleration voltage of 20 kV, sample tilt angle of 70°, working distance of 12 mm and 0.3 μm step size. The HKL Technology Channel 5 and MTEX software were used to analyze and display the EBSD data.

3. Results and discussion

Fig. 1 shows the SEM image by secondary electrons and XRD diffraction pattern of the investigated Maraging sample. Only body-centered cubic martensite (α-BCC) was detected by XRD. This can be explained by low tetragonal BCC martensite developed in Maraging steels because carbon atoms cannot occupy the octahedral positions in austenitic structure in low carbon content (< 0.02%) steels [19–21]. In addition, SEM image shows distinct well-etched and less etched regions. Well-etched regions are associated by tempered martensite formed under the first quenching. However, fresh martensite formed during the second quenching with (slightly) higher carbon content because of carbon depleted due to carbon ejection from firstly martensite [22]. The hardness and prior austenite grain size were measured as 650 ± 25 HV and 34 ± 6 μm, respectively. It is worth mentioning that the dispersion of fresh martensite through the very low tetragonal tempered martensite improved mechanical behaviour (increasing both strength and ductility, simultaneous) [23,24].

Table 1
Chemical analysis of investigated samples (in wt%).

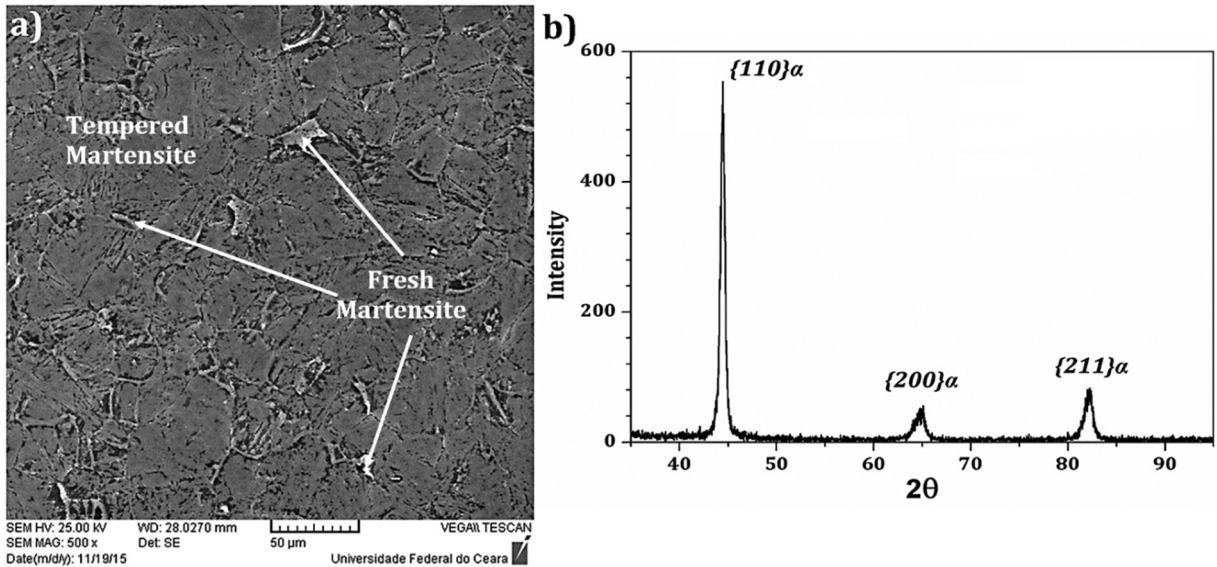| Ni	Co	Mo	Ti	Al	Si	C	Fe
18.23	11.64	4.86	1.38	0.07	0.07	0.01	Bal.

Fig. 1. (a) SEM micrographs and (b) X-ray diffraction pattern of high strength 350 Maraging steel.

Some microcracks that led to early failure were initiated and propagated through the investigated sample, and they are shown in Fig. 2. Transgranular crack propagation is dominant in this sample, however, some intergranular crack propagations were also observed. The crack nucleation mostly appears to be partly intergranular whereas propagation seems to assume mainly a transgranular pathway. Mohtadi-Bonab et al. [25] also reported the dominance of transgranular crack propagation manner due to a high stress concentration factor because of formation of micro-shear bands. In addition, Zhu et al. [26] suggested that transgranular cracking was associated with both microshear on the {111} planes and microcleavage mainly on the {100} planes, as well. Energy-dispersive X-ray spectroscopy (EDS) analysis was carried out close to the cracks to characterize probable alloying segregation. However, no evidence was found for micro-alloying segregation and the presence of precipitation to explain failure in this sample (Fig. 3). Therefore, EBSD analyses were employed to explain the crack formation/propagation.

EBSD analyze was employed to characterize the influence of grain orientation and distribution of boundary types to reveal their effects on enhance/prevent cracks propagation. The normal direction orientation images microscopy (OIM) in different regions (i.e., contained cracks and free-crack regions) is presented in Fig. 4. Low angle boundaries (LABs) are shown with thin lines. However, high angle boundaries (HABs) corresponded to have higher dislocation densities and higher stored energy shown by thick lines. EBSD data also revealed that both transgranular and intergranular crack propagations are responsible for the early failure of the specimen. The crystallographic texture and grain-boundary engineering have been attracted a lot of attention to increase the hydrogen embrittlement resistance by providing resistant paths for crack propagation. Mohtadi-Bonab et al. [27] reported that some dominant textures (such as {111}, {112}, and {110} parallel to rolling direction) fibers might reduce the hydrogen embrittlement susceptibility by
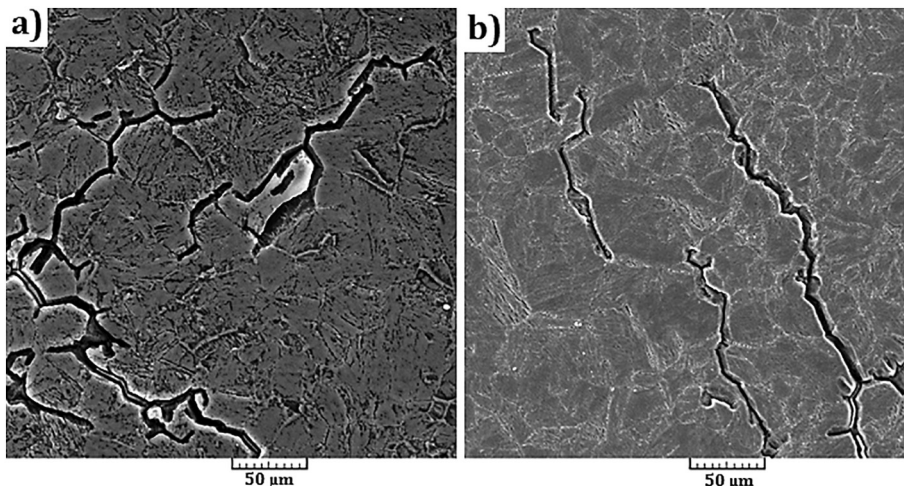

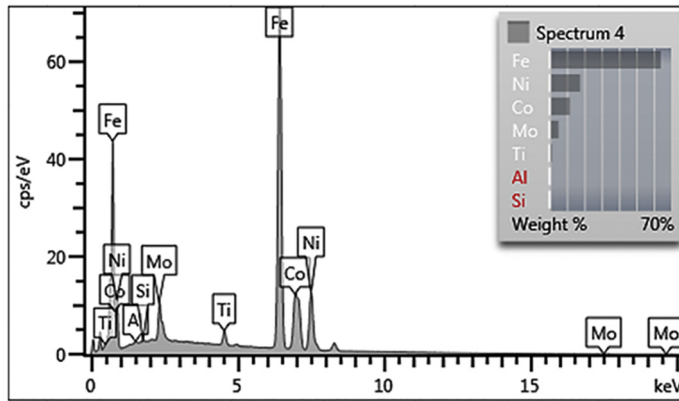**Fig. 2.** SEM micrograph of cracked regions of investigated sample.

Fig. 3. EDS result of the elemental compositions in the vicinity of crack paths.
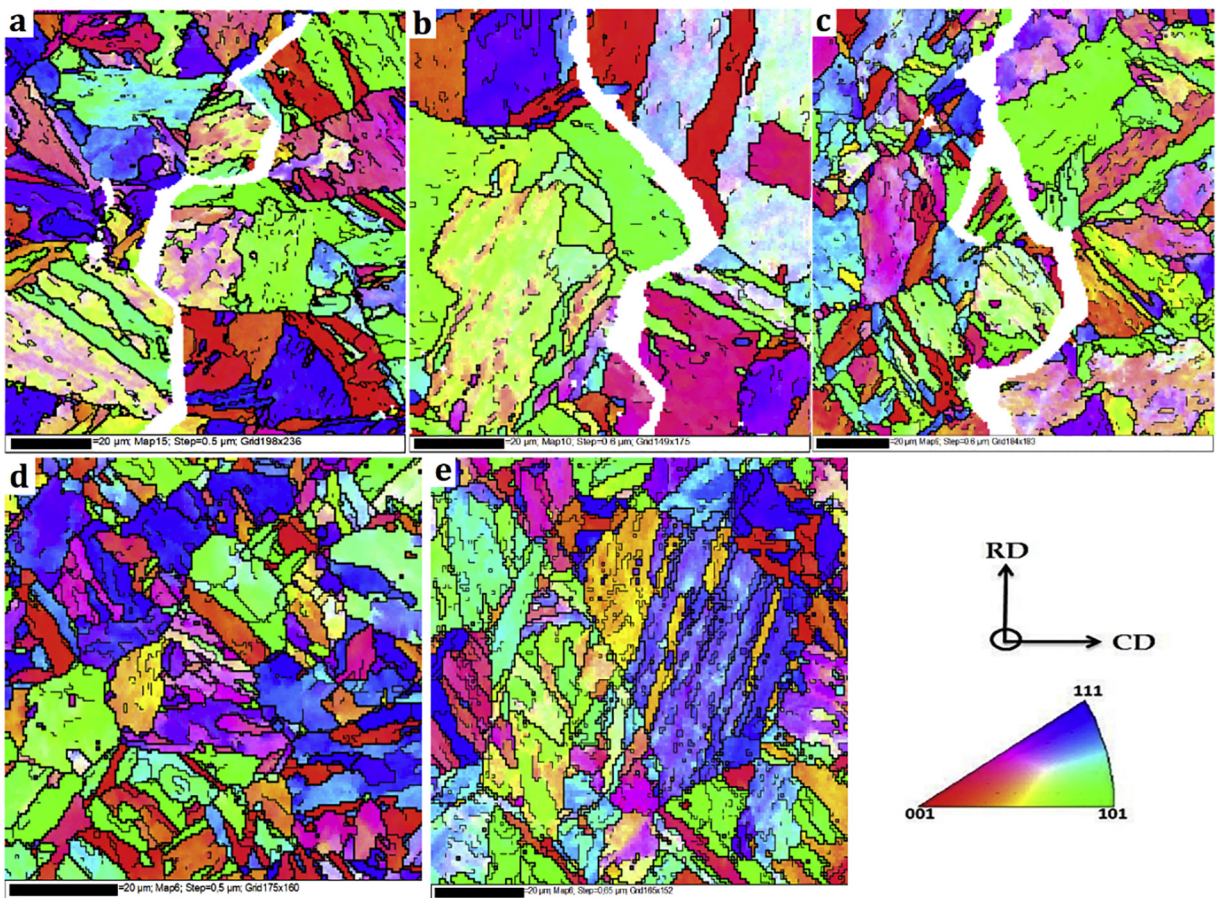

Fig. 4. OIM maps of different regions with/without cracks.

decreasing the number of both intergranular and transgranular paths. The formation of low energy boundaries such as coincidence site lattice (CSL) boundaries and LABs can also increase the intergranular crack resistance [28]. Meanwhile, very fine intermetallic precipitates in maraging steels (such as $Ni_3(Ti,Mo)$) that play significant role in increasing the mechanical resistance by precipitation hardening, avoid the formation of stress concentration and also act as obstacle for crack propagation [29].

Furthermore, the improvement in the crack resistant is notable in areas with higher number of LABs due to the higher density of dislocations in martensitic structure. The grain boundaries or HABs formed as a result of recrystallization which enhances atoms mobility and diffusion paths into solution, might accelerate the strain aging and crack nucleation [30]. Moreover, the strong cleavage {100} parallel to normal direction formed as a result of recrystallization in these steels, deteriorating ductility [21]. On the other
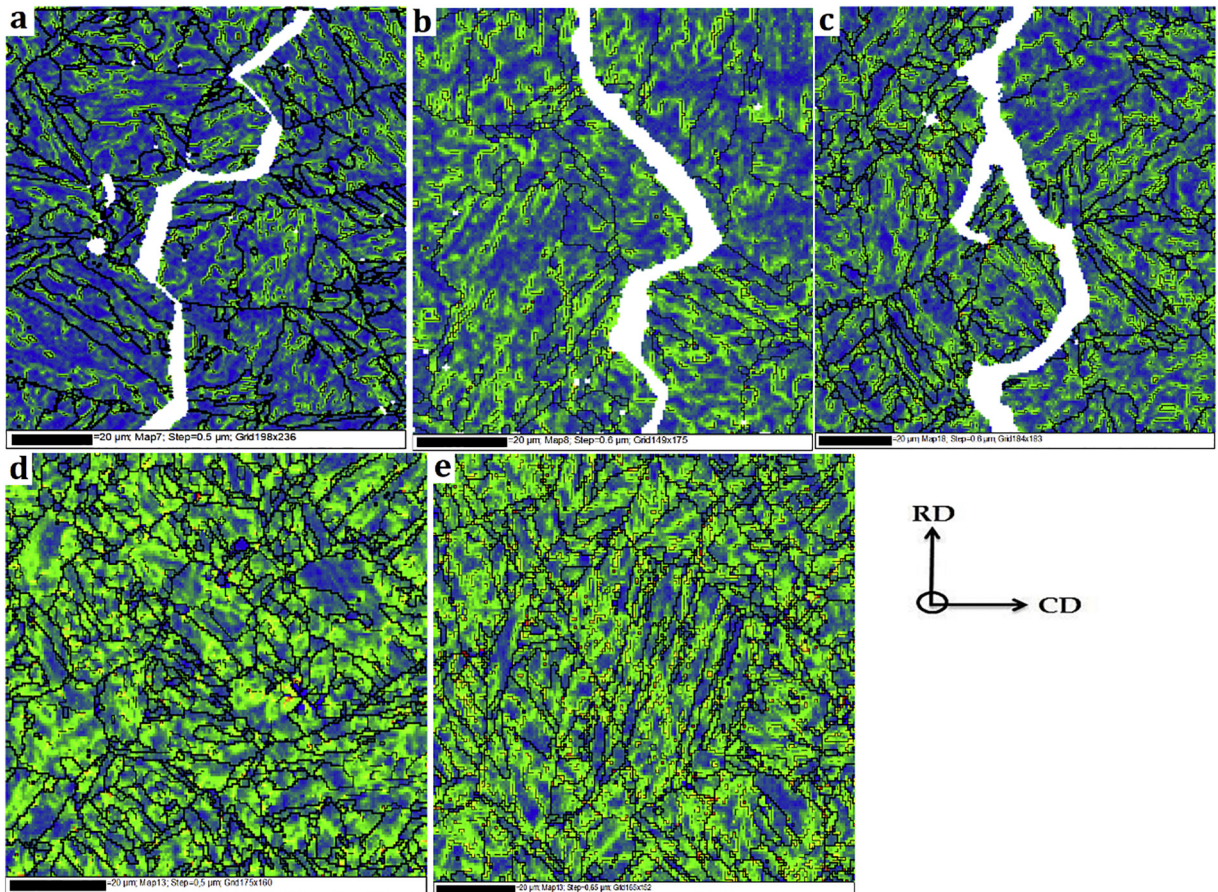
Fig. 5. KAM maps of different regions with/without cracks.

hand, recovery releases the stored energy by dislocations annihilation and rearrangement providing subgrains accompanied with secondary precipitation improving crack nucleation and/or propagation resistance.

Kernel average misorientation (KAM) analyze was measured to show the heterogeneous plastic deformation in every grain [31,32]. KAM maps in different regions are shown in Fig. 5. KAM quantifies the average misorientation or local distortion of an individual grain with respect to crystallographic changes inside the grain. The result showed that local deformation was concentrated in the vicinity of crack paths. In contrast, the local deformation in free-cracked regions was well distributed among all grains. In other words, local plastic deformation was concentrated at the crystalline defect, led to accelerating crack propagation. However, distribution of plastic deformation along various grains prevented the occurrence of localized plastic deformation. Grain boundaries and crystallographic defects increase the number of tangles of immobile dislocations (dislocation piles-up), leading to increasing instability by cumulative the stored energy.

Taylor introduced the classical plasticity theory to describe polycrystalline materials deformation at micron level [33,34]. It is well-known that the plastic deformation of a material depends not only on the strain, but also depends on the stress state, strain gradient, and grains orientation. Von Mises [35] assumes that at least five active slip systems are required to accommodate the plastic deformation. In addition, according to Taylor factor each grain deforms individually in the manner of the polycrystalline aggregation by respecting the deformation continuity through the grain boundaries [33,34]. Low Taylor factor grains are considered as soft grains with relatively low indication of strain hardening and easy to deform. However, high Taylor factor grains as hard grains with high indication of strain hardening, acts to be more resistant to deform plastically. On the one hand, high Taylor factor grains cannot plastically deform, leading to promote lattice discontinuity at grain boundaries [36]. On the other hand, low Taylor factor (soft) grains tend plastically deform without reorientation, while lattice incompliance and stress concentration increase at grain boundaries. Therefore, stress concentration at grain boundaries promotes crystallographic defects (such as microcrack) and provide easy path to its propagation, Fig. 6a–c. In other words, dislocations generated during plastic deformation pass through the material and piles-up due to the crystalline defect and orientation gradients (mismatch of slip directions at grain boundaries). Accumulations of dislocations obstruct the motion of other moving dislocations, causing work hardening and strain concentration. Thus, these hard grains finally fragment because of high localized strain concentration. However, soft grains with adequate activated slip systems facilitate dislocation movements and impede dislocation accumulation, Fig. 6d–e.

Although OIM color maps present the variation of crystal orientations, it has an unavoidable limitation based on the Euler scheme
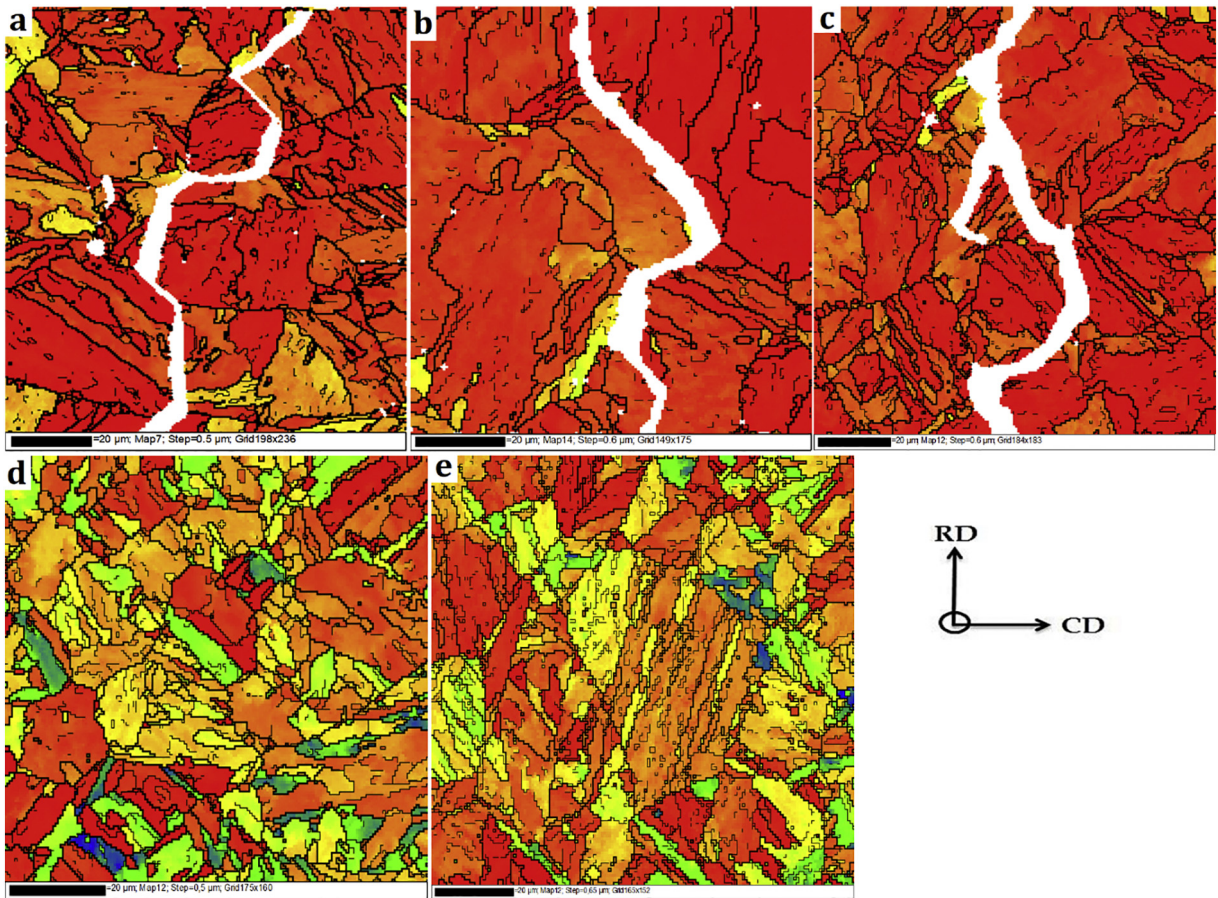
Fig. 6. Taylor maps of different regions with/without cracks.

[37]. Therefore, to calculate the high orientation precision of orientation distribution in cracked and cracked-free regions, an inverse pole figure (IPF) was calculated based on Kernel density estimation and presented as maps in Fig. 7. {012} crystallographic textures were characterized in both regions. Hu [38] reported that these textures were developed during warm deformation due to the number of slip and twinning systems with the low crystal symmetry, leading to the development of non-randomness of the grain orientations. In contrast {113} crystallographic textures were dominant in the vicinity of crack path, however, {122} textures were developed in non-cracked regions. Azar et al. [13] also reported the formation of {113} grains parallel to normal direction on the crack extension. It was observed that {012}-{113} crystallographic textures have been arranged approximately 25.5° deviation from the {001} textures, and the {012}-{122} have been arranged around the {110} texture with approximately 18.5° deviation. In BCC structure, {011} planes are known as the most compacted planes with the nearest interatomic distance, leading to facilitate dislocation movements by slip mechanism. Thereby, it could be explained the better local strain gradient and lower Taylor factor grains in non-
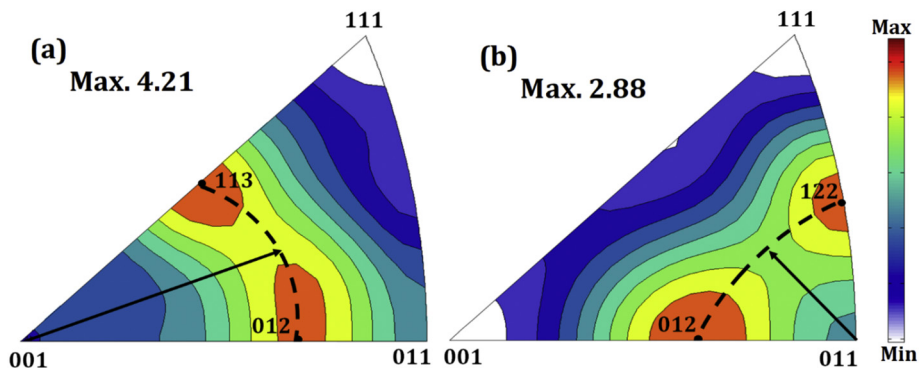

Fig. 7. Inverse pole figure maps of (a) cracked and (b) non-cracked regions calculated from EBSD data.
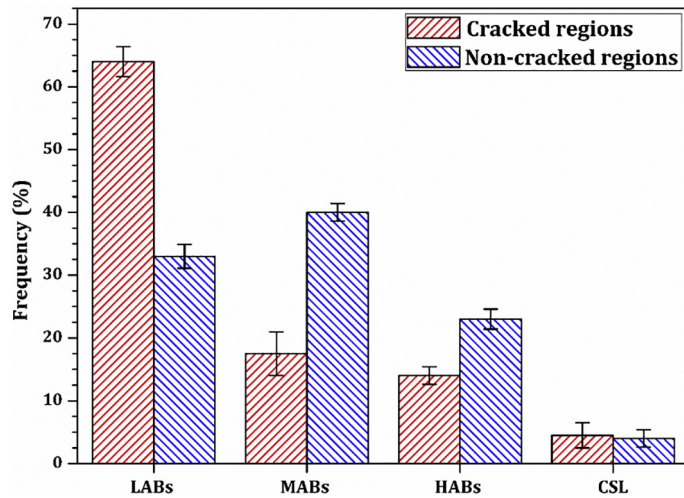
Fig. 8. Distribution of grain boundaries of two cracked and non-cracked regions calculated from EBSD data.

cracked areas. However, {001} planes are the least closed pack planes and the largest interatomic distance impede dislocation motion, causing dislocation piles-up and increasing internal energy. Consequently, crack formation and early failure are expected.

It is well-known that the grain boundary character distribution in a material plays a significant role in mechanical properties due to storage of array of dislocation or crystalline defects [31,39,40]. EBSD technique cannot detect crystal defects (such as voids, dislocation, etc), however, this method can determined their effects on lattice distortion. LABs (low angle boundaries) are identified by point-to-point misorientations of neighbouring crystals between 2 and 5°. Medium angle boundaries or subgrain boundaries (MABs, point-to-point misorientations between 5° and 15°) and HABs (point-to-point misorientations > 15°) were determined, respectively. To study the effect of the type of grain boundaries / misorientation on the susceptibility to crack propagation, grain boundary misorientation was calculated from the average of cracked and un-cracked regions (3 areas, x 250) which were contained around 187 grains. Fig. 8 shows the distribution of grain boundary types in two distinct regions with and without crack propagations. A high fraction of LABs indicated a high number of dislocation tangles and accumulation of dislocation, which was settled at dislocation walls, leading to increase the instability of lattice compliance. However, this lattice in-conformability could relieve due to dislocation rearrangement and annihilation by recovering according to the dislocation mobility discussed earlier. It led to avoid formation of strain localization, as a consequent, prevent crack initiation. Special boundaries with random boundaries act as LABs with low internal energy played an ignorable role on crack formation in this sample.

In the present paper, microstructural features were analyzed using SEM, XRD, and EBSD technique conducted to show the importance of grain orientation and grain boundary characteristics in severe environment. Although, detailed microstructure containing the tempered low tetragonal martensite and fresh martensite were characterized by SEM. No microstructure and precipitates correlation were found for crack initiation and propagation. EBSD revealed detailed information of final substructure, such as grain orientation, grain boundary types, distribution of local strain gradient, and crystallographic defect. The results showed that the development of grains approximate the most compact {110} planes promotes dislocation mobility by providing adequate slip systems, avoiding formation of strain concentration and micro-crack initiation. However, hard grains or high Taylor factor grains due to low insufficient slip systems, lead to increasing dislocation accumulation and lattice distortion. The formation of high number of LABs with meaningful stored energy facilitates micro-crack initiation or provides preferred sites for crack propagation. The crystallographic data analyses were obtained from EBSD data and discussed previously, summarized in Table 2.

Table 2
Summery of crystallographic data analyzing contained KAM, Taylor factor, and boundary distributions.

Parameter	Description	Cracked regions	Non-cracked regions
Kernel average misorientation (KAM)	Low Kernel (KAM < 1°)	53 ± 5.0	15 ± 3.0
	Moderate Kernel (1° < KAM < 4°)	44 ± 5.0	75 ± 3.0
	High Kernel (KAM > 4°)	3 ± 2.5	7 ± 1.5
Taylor factor	Low Taylor (TF < 1)	2.1 ± 0.5	17.7 ± 2.5
	Moderate Taylor (1 < TF < 3)	23.7 ± 2.5	48.00 ± 2.5
	High Taylor (TF > 3)	74.2 ± 3.0	34.3 ± 2.5
Boundary distribution	LABs (0–5)	64.0 ± 2.5	33.5 ± 2.5
	MABs (5–15)	17.5 ± 2.5	40.0 ± 2.5
	HABs (15–62)	14.0 ± 2.5	23.0 ± 2.5
	CSL	5.0 ± 2.5	4.5 ± 2.5

4. Conclusions

Microstructure features were studied in a fractured elbow Maraging steel which was used in parts operating under stress in an environment with traces of hydrofluoric acid. The aim of this work was to characterize the failure behaviour and show the importance of crystallographic features on failure analyses. Following conclusions are summarized as follows:

- Two martensite structure were characterized by SEM; (i) tempered low tetragonal martensite (well-etched area), (ii) fresh martensite (less etched regions).
- Grains oriented along {110} crystallographic texture with approximately 18.5° deviation can be provide adequate slip systems to distribute dislocation and avoiding microcrack formation.
- High Taylor factor value increased lattice incompliance increased dislocation piles-up, leading to initiation microcrack.

Acknowledgement

References

[1] C.G. Bieber, J.R. Mihalisin, Progress toward Attaining Theoretical Strength with Iron-Nickel Maraging Steels, JOM1, vol. 18, (1966), pp. 1033–1036.
[2] R.D. Jones, D. Rowlands, P.L. Rossiter, Resistivity changes during maraging processes in iron-nickel steels, Scr. Metall. 5 (1971) 915–920.
[3] X. Li, Z. Yin, Reverted austenite during aging in 18Ni (350) maraging steel, Mater. Lett. 24 (1995) 239–242.
[4] A.C. Rodrigues, H.H. Bernardi, J. Otubo, Microstructural analysis of co-free Maraging steel aged, J. Aerosp. Technol. Manag. 6 (2014) 389–394, https://doi.org/10.5028/jatm.v6i4.400.
[5] Y. He, K. Yang, W. Qu, F. Kong, G. Su, Strengthening and toughening of a 2800-MPa grade maraging steel, Mater. Lett. 56 (2002) 763–769.
[6] H. Leitner, M. Schober, R. Schnitzer, S. Zinner, Strengthening behavior of Fe-Cr- Ni-Al-(Ti) maraging steels, Mater. Sci. Eng. A 528 (2011) 5264–5270, https://doi.org/10.1016/j.msea.2011.03.058.
[7] G. Malakondaiah, M. Srinitlas, P.R. Raot, Ultrahigh-strength steels with enhanced fracture toughness, Prog. Mater. Sci. 42 (1997) 209–242.
[8] Z.B. Jiao, J.H. Luan, M.K. Miller, Y.W. Chung, C.T. Liu, Co-precipitation of nanoscale particles in steels with ultra-high strength for a new era, Mater. Today 20 (2017) 142–154.
[9] A.G.F. Padial, W. Monteiro, A.H. Andrade, O. Rigo, Microstructural Analysis of 400 Grade Maraging Steel After Thermomechanical Teratment, (2019).
[10] M. Masoumi, L.P.M. Santos, I.N. Bastos, S.S.M. Tavares, M.J.G. da Silva, H.F.G. de Abreu, Texture and grain boundary study in high strength Fe-18Ni-Co steel related to hydrogen embrittlement, Mater. Des. 91 (2016) 90–97, https://doi.org/10.1016/j.matdes.2015.11.093.
[11] M. Masoumi, M. Béreš, L. Wu, L.P.M. Santos, F.A.M. da Rocha Filho, C.C. da Silva, H.F.G. de Abreu, M.J. Gomes da Silva, Role of lattice strain and texture in hydrogen embrittlement of 18Ni (300) maraging steel, Int. J. Hydrog. Energy 42 (2017) 14786–14793, https://doi.org/10.1016/j.ijhydene.2017.03.209.
[12] N.C. Figueiredo, C.A.S. de Oliveira, M. Masoumi, H.F.G. de Abreu, Microstructural variations at different distance from the surface in forged 18 Ni C300 maraging steel, J. Mater. Res. Technol. (2018) 1–8, https://doi.org/10.1016/j.jmrt.2018.01.007.
[13] A.S. Azar, L.E. Svensson, B. Nyhus, Effect of crystal orientation and texture on fatigue crack evolution in high strength steel welds, Int. J. Fatigue 77 (2015) 95–104, https://doi.org/10.1016/j.ijfatigue.2015.03.008.
[14] R. Blondé, E. Jimenez-Melero, L. Zhao, J.P. Wright, E. Brück, S. Van Der Zwaag, N.H. Van Dijk, High-energy X-ray diffraction study on the temperature-dependent mechanical stability of retained austenite in low-alloyed TRIP steels, Acta Mater. 60 (2012) 565–577, https://doi.org/10.1016/j.actamat.2011.10.019.
[15] A. Kedharnath, A.S. Panwar, R. Kapoor, Molecular dynamics simulation of the interaction of nano-scale cracks with grain boundaries, Comput. Mater. Sci. 137 (2016) 85–99.
[16] A.J. Wilkinson, A new method for determining small misorientations from electron back scatter diffraction patterns, Scr. Mater. 44 (2001) 2379–2385.
[17] A.J. Wilkinson, P.B. Hirsch, Electron diffraction based techniques in scanning electron microscopy of bulk materials, Micron. 28 (1997) 279–308.
[18] W. Osborn, L.H. Friedman, M. Vaudin, Ultramicroscopy strain measurement of 3D structured nanodevices by EBSD, Ultramicroscopy J. 184 (2018) 88–93.
[19] D. Ponge, H. Assadi, M. Herbig, P. Choi, J. Milla, Segregation engineering enables nanoscale martensite to austenite phase transformation at grain boundaries: a pathway to ductile martensite, Acta Mater. 61 (2013) 6132–6152.
[20] S.H. Nedjad, M.N. Ahmadabadi, T. Furuhara, Correlation between the intergranular brittleness and precipitation reactions during isothermal aging of an Fe-Ni-Mn maraging steel, Mater. Sci. Eng. A 490 (2008) 105–112, https://doi.org/10.1016/j.msea.2008.01.070.
[21] M. Masoumi, I.F. de Barros, L.F.G. Herculano, H.L.F. Coelho, H.F.G. de Abreu, Effect of microstructure and crystallographic texture on the Charpy impact test for maraging 300 steel, Mater. Charact. 120 (2016) 203–209, https://doi.org/10.1016/j.matchar.2016.09.003.
[22] D. De Knijf, R. Petrov, C. Föjer, L.A.I. Kestens, Effect of fresh martensite on the stability of retained austenite in quenching and partitioning steel, Mater. Sci. Eng. A 615 (2014) 107–115, https://doi.org/10.1016/j.msea.2014.07.054.
[23] A. Schulz-beenken, Martensite in steels : its significance , recent developments and trends, J. Phys. IV Colloq. 07 (1997) 359–366.
[24] C.G. Norwood, The Effect of Nickel Content on the Mechanical Properties and Microstructure of a High Toughness Secondary Hardening Steel, (2016), https://doi.org/10.1109/UUST.1980.1158402.
[25] M.A. Mohtadi-Bonab, M. Eskandari, M. Sanayei, S. Das, Microstructural aspects of intergranular and transgranular crackpropagation in an API X65 steel pipeline related to fatigue failure, Eng. Fail. Anal. 94 (2018) 214–225.
[26] L. Zhu, Y. Yan, J. Li, L. Qiao, Z. Li, A.A. Volinsky, Stress corrosion cracking at low loads : surface slip and crystallographic analysis, Corros. Sci. 100 (2015) 619–626.
[27] M.A. Mohtadi-Bonad, M. Eskandari, J.A. Szpunar, Effect of arisen dislocation density and texture components during cold rolling and annealing treatments on hydrogen induced cracking susceptibility in pipeline steel, J. Mater. Res. 31 (2016) 3390–3400, https://doi.org/10.1557/jmr.2016.357.
[28] M.A. Mohtadi-Bonab, M. Eskandari, H. Ghaednia, S. Das, Effect of microstructural parameters on fatigue crack propagation in an API X65 pipeline steel, J. Mater. Eng. Perform. 25 (2016) 4933–4940, https://doi.org/10.1007/s11665-016-2335-6.
[29] K. Li, L. Wei, B. An, B. Yu, R.D.K. Misra, Aging phenomenon in low lattice-mis fi t cobalt-free maraging steel : microstructural evolution and strengthening behavior, Mater. Sci. Eng. A 739 (2019) 445–454.
[30] X. Xu, S. Ganguly, J. Ding, P. Dirisu, F. Martina, X. Liu, S.W. Williams, Improving mechanical properties of wire plus arc additively manufactured maraging steel through plastic deformation enhanced aging response, Mater. Sci. Eng. A 747 (2019) 111–118.
[31] P.J. Konijnenberg, S. Zaefferer, D. Raabe, Assessment of geometrically necessary dislocation levels derived by 3D EBSD, Acta Mater. 99 (2015) 402–414, https://doi.org/10.1016/j.actamat.2015.06.051.
[32] M. Calcagnotto, D. Ponge, E. Demir, D. Raabe, Orientation gradients and geometrically necessary dislocations in ultrafine grained dual-phase steels studied by 2D

and 3D EBSD, Mater. Sci. Eng. A 527 (2010) 2738–2746, https://doi.org/10.1016/j.msea.2010.01.004.

[33] G.I. Taylor, Mathematical and physical sciences the deformation of crystals of β-brass, Proc. R. Soc. A Math. Phys. Eng. Sci. IV (1927) 167–188.

[34] G.I. Taylor, C.F. Elam, The distortion of Iron crystals, Proc. R. Soc. A Math. Phys. Eng. Sci. 112 (1926) 337–361, https://doi.org/10.1098/rspa.1926.0116.

[35] R. von Mises, Mechanics of solid bodies in the plastically-deformable state, J. Appl. Math. Phys. 1 (1913) 582–592.

[36] S. Birosca, The deformation behaviour of hard and soft grains in RR1000 nickel-based superalloy, IOP Conf. Ser. Mater. Sci. Eng. 82 (2015) 15–21, https://doi.org/10.1088/1757-899X/82/1/012033.

[37] G. Nolze, Euler angles and crystal symmetry, Cryst. Res. Technol. 201 (2015) 188–201, https://doi.org/10.1002/crat.201400427.

[38] H. Hu, Texture of metals, Texture, Gordon and Breach Science Publishers Ltd., United Kingdom, 1974, pp. 233–258.

[39] T. Maitland, S. Sitzman, EBSD technique and materials characterization examples.pdf, Scanning Microsc. Nanotechnol. Tech. Appl. (2007) 41–76.

[40] C. Moussa, M. Bernacki, R. Besnard, N. Bozzolo, About quantitative EBSD analysis of deformation and recovery substructures in pure Tantalum, IOP Conf. Ser. Mater. Sci. Eng. 89 (2015), https://doi.org/10.1088/1757-899X/89/1/012038.